Respiratory Pattern Recognition from Low-Resolution Thermal Imaging

Salla Aario[1], Ajinkya Gorad[1], Miika Arvonen[2], and Simo Särkkä[1] *

1- Aalto University - Dept. of Electrical Engineering and Automation
Otakaari 3, Espoo, Finland

2- Kuopio University Hospital - Dept. of Paediatrics
Puijonlaaksontie 2, Kuopio, Finland

Abstract. Remote monitoring of vital signs has a wide range of applications. In this paper we propose a method to identify respiratory patterns from low-resolution thermal video data using a nearest neighbor data association (NNDA) and nearest neighbor Kalman filter (NNKF) based algorithms along with multi-class support vector machine (SVM). The method in this work is evaluated against breathing belt data as a reference, collected from healthy volunteers. Correlation of the proposed method with airflow derived from the breathing belt was found to be 0.7. The SVM classifier is able to distinguish between the breathing patterns from derived airflow with 60% accuracy.

1   Introduction

This paper is concerned with the measurement of breathing patterns using non-contact thermal imaging. The aim is to develop a new computer vision based methodology for processing of the thermal images in order to produce a measurement of respiration. Accurate measurement of respiration plays an important role in assessing and treating several respiratory disorders. These disorders are commonly identified by changes in the respiratory rate (RR), abnormal changes in breathing volume, or changes in respiratory sounds. A raised or irregular RR has also been shown to be a strong predictor of serious clinical events, such as cardiac arrest, meaning that monitoring of respiratory rate is very important for patient assessment [1, 2].

Methods of measuring respiratory function can be divided into two categories - contact and non-contact [3]. In contact respiratory function monitoring, the instrument makes direct contact with the subject's body, whereas in non-contact monitoring there is no direct contact with the body. There have been numerous studies on both monitoring methods, as reviewed by Folke et al [4]. Non-contact assessment of breathing function has been of growing interest in the past two decades due to its advantages - for example, monitoring of infants or monitoring severely burnt patients. The use of thermal imaging to measure respiratory rate has been introduced in several studies (e.g. [5–10]). Thermal imaging is a remote non-contact monitoring method, with a passive nature – it does not

---

supply current or emit radiation to the patient but it measures the natural heat radiation of the target. It is independent from illumination, making it useful in sleep studies.

The contribution of this article is to develop a new method which uses remote, non-contact low-resolution thermal imaging to track, recognize, and classify different breathing patterns. The temperature of each nostrils is measured separately, and each nostril is tracked based on the thermal feature of breathing. We also developed a thermal model to estimate the airflow through the nostrils. A respiratory belt was used as a gold-standard reference method. In contrast with earlier studies [11, 12], we processed the thermal signal using a nearest neighbour data association algorithm to track the individual nostrils over the image sequences. Previous studies have also mainly concentrated on recognizing only the respiratory rate [13] however our method is also capable of detecting different types of respiratory disorders.

2   Materials and Methods

2.1   Setup and Dataset

Setup involved a healthy human volunteer, the Samsung Galaxy S9 Smartphone with the FLIR ONE Pro Thermal Camera [14] to record thermal video, Bionomadix breathing belt with MP150 data acquisition system interface by BIOPAC for validating the thermal measurements, and a laptop for recording and processing the data offline. A custom developed Android app with the FLIR ONE SDK was used to retrieve the thermal raw frames from the FLIR sensor and stream it to Matlab.

To simulate different breathing patterns with the help of healthy volunteers, a custom Breath Dictator (BD) software was used. BD supplies a supervisory stimuli through a display screen which helps mimic different breathing patterns for the volunteer. These stimuli were displayed in the Matlab GUI where breathing was denoted by a marker on a 2D amplitude vs time. Overall 4 BD sequences were formed which consisted of nine breathing patterns : Eupnea (E), Tacypnea (T), Kussmaul (K), Apnea (A), Cheyne–Stokes (C), Moderate obstructed (M), Severe obstructed (S), Plateau after inhale-exhale (P), and Nasal Flaring (N). These sequences were validated by a medical doctor. A similar approach was adopted in [11, 12].

Using the BD and the FLIR camera [14], four samples each from two subjects were recorded for each BD sequence, resulting in 16 samples for each subject. Each sample recording consisted of thermal video of the face together with breathing belt data. Each thermal recording had a mean sampling rate of about 4 Hz with raw thermal frames of 160×120 pixels.

2.2   Image processing

During inhale and exhale, significant temperature changes are visible in the nostrils. Otherwise the temperature profile of the face is relatively static. During

inhale, the inside of the nostrils gets cooler due to surrounding cold air imping-ing on its surface. This allows simple image processing techniques to extract the location of the nostrils without the use of complex methods like face and feature recognition, which may require higher resolution [11, 12]. For each frame of thermal video, a window is chosen from the first frame which remains static for its subsequent frames. Each image is smoothed with a 2D Gaussian filter of variance 0.5. Then, the morphological operation of filling holes in an inten-sity image is used. It fills the pixel-area of lower temperature surrounded by higher temperature with the surrounding higher temperatures. The filled image is subtracted from the smoothed image providing cold spots surrounded by high temperature. During inhale the two nostrils show relatively drastic temperature differences and are the most prominent cold spots. Hence the local maxima of intensity in the cold spot image gives the potential nostril locations.

2.3   Data association algorithms

From the list of potential nostril locations, trajectory of nostrils is calculated, first using nearest neighbour data association (NNDA), and second with a near-est neighbour Kalman filter (NNKF) algorithm. At each time step, the pixel locations and their temperature values for the first $n = 2$ local maxima values are retained for the cold spot frame. This gives a list of potential nostril locations which needs to be tracked. A heuristic threshold is calculated as the average of the min-max value of the maximum of each cold spot frame. The positions corre-sponding to the local maxima values from cold spots frames above the threshold were considered as detections and the frames with no clear cold spots (below the threshold) where considered as missing measurements in the tracker. Near-est neighbour data association algorithm [15] using Euclidian norm was used only for these frames to track the locations in the list. The nostril locations were then linearly-interpolated in between the inhale frames, and zeroth-order-interpolated out of the frames. From these interpolated nostril locations, the thermal signal is looked up from the original image sequence. As an alternative method for NNDA, we also used the Kalman filtering (KF) based nearest neigh-bour data association method [15] to track the nostril position sequence taking below-threshold values as missing measurements of position.

2.4   Airflow prediction

The breathing belt is used for validating the respiratory measurements from the thermal camera. Their recorded signals were synchronized and re-sampled to 1 kHz. In this work, a reference approximate airflow was computed as the time derivative of the belt signal. Since the breathing belt provides the displacement of chest perimeter, changes in volume of the lungs can be approximated to be proportional to change in the perimeter. This airflow like quantity (α_v) is used to model inside-the-nostril surface temperature (T). During inhale the cold surrounding air impinges on the nasal passage, cooling it, while when warm air comes out of the lungs during exhale, the nostril skin temperature rises quickly.

When there is no exchange of air, the temperature rises to body temperature relatively slowly. Hence, the simplified model for this phenomena is:

$$\frac{\mathrm{d}T}{\mathrm{d}t} = -\lambda(T - \theta)|\alpha_v(t)| - \kappa(T - M), \tag{1}$$

which allows us to solve for $\alpha_v(t)$ as function of T and $\mathrm{d}T/\mathrm{d}t$.

Above, the target temperature θ is due to the surroundings on inhale, and inside of the body on exhale. It has $\lambda \, (= 1)$ as the decay constant for airflow-induced temperature change. The target temperature to which T rises without any airflow is taken as $M = 1 + \max(|\Delta T|)$, where $|\Delta T|$ is the maximum temperature deviation of nostrils from the face, and $\kappa \, (= 0.5)$ is the decay constant for heat conduction to surrounding skin. The derivative of thermal signal was estimated with a Kalman smoother with a Wiener velocity model [16, 17].

2.5   Classification of breathing patterns

The airflow predictions are resampled to 20 Hz and a Kalman-smoother-based time-frequency spectrogram [18] (frequencies from 1/60 Hz to 80/60 Hz with step of 1/60 Hz) is computed for all samples. The approximate number of feature vectors for each class was taken to be 8000 to make a balanced distribution. The single-time spectrograms slices of the first subject were used as the inputs to the classifier and the aim was to predict the class labels of second subject and vice versa, achieving twofold classification. We used an error-correcting output codes (ECOC) classifier (see, e.g., [19]) with support vector machine (SVM) as the binary classifier.

3   Results and Discussion

In this section we present the experimental result for the proposed method. For comparison, we also computed the average signal over a rectangular window called Region of Interest (ROI) covering both the nostril locations. This methodology was adopted in [11] to compute the respiratory signal and is used to compare the classification performance of single pixel measurements of nostril thermal data from this work.

A single recording of belt and thermal camera measurements from the same session and subject is shown in Fig. 1. Clear differences in belt signals and thermal signals can be seen for different breathing patterns. The temperature curves were evaluated using NNDA, NNKF, and ROI methods and the airflow model in Equation (1). Major differences are visible in case of tachypnea (T) and respiration with plateau (P). In particular two decays timescales can be seen from the breath-in, hold and breath out. The correlations between the airflow derived from the breathing belt with the thermal camera based estimates were the following: NNDA = 0.72, NNKF = 0.66, ROI = 0.54. Also, both nostrils have different temperatures with one nostril having (for NNDA and NNKF) approximately 1.4× higher temperature than the other, likely due to different airflow from each nostril.
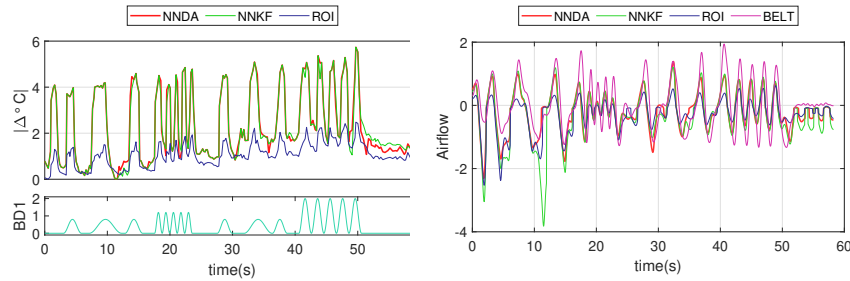
Fig. 1: Left: an example of breath dictator sequence and the extracted thermal signals. Right: airflow signals obtained from Equation (1).

Spectrograms of the airflow signals in Fig. 1 and the confusion matrix for SVM classification are given in Fig. 2. The classification accuracies are: NNDA = 60%, NNKF = 52%, ROI = 47%, and BELT = 62%. That is, the accuracy of NNDA is very close to that of the breathing belt and the accuracy of NNKF is slightly lower. The accuracy of the ROI-based method is the lowest of all methods. From the confusion matrix of NNDA it can be seen that the breath types N and P, which both have plateau after inspirium and expirium, are mixed with each other. Most breathing patterns are not separable in the ROI method.
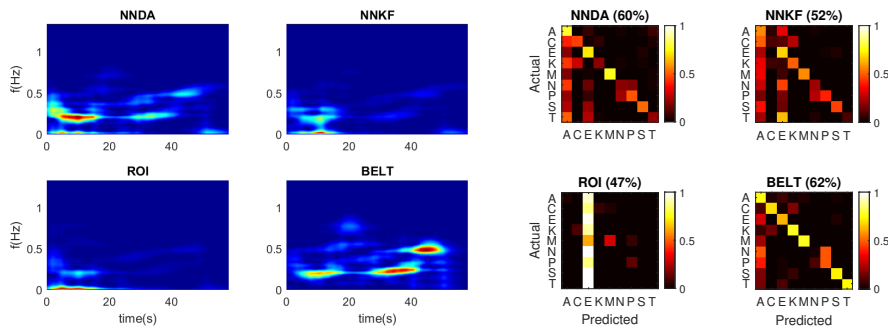

Fig. 2: Left: spectrograms obtained from the airflows in Fig. 1. Right: confusion matrices for the breathing patterns (from all the data).

4   Conclusion

In this paper, we have presented an algorithm to track the nostril locations and extract the temperature signal using a low resolution thermal camera. We have also shown how the breathing patterns can be automatically classified based on this information. We compared the method to the gold standard of a breathing belt and a reference method. The results suggest that it is possible to identify various breathing patterns remotely using a thermal camera.

References

[1] M.A. Cretikos, R. Bellomo, K. Hillman, J. Chen, S. Finfer, and A. Flabouris. Respiratory rate: the neglected vital sign. *Med J Australia*, 188(11):657–659, 2008.

[2] J.F. Fieselmann, M.S. Hendryx, C.M. Helms, and D.S. Wakefield. Respiratory rate predicts cardiopulmonary arrest for internal medicine patients. *J Gen Intern Med*, 188:354–360, 1993.

[3] F.Q. Al Khalidi, R. Saatchi, D. Burke, H. Elphick, and S. Tan. Respiration rate monitoring methods: A review. *Pediatric Pulmonology*, 46(6):523–529, 2011.

[4] M. Folke, L. Cernerud, M. Ekström, and B. Hök. Critical review of non-invasive respiratory monitoring in medical care. *Med Biol Eng Comput*, 41(4):377–383, Jul 2003.

[5] R. Murthy and I. Pavlidis. Noncontact measurement of breathing function. *IEEE Eng Med Biol*, 25(3):57–67, 2006.

[6] J.N. Murthy, J. van Jaarsveld, J. Fei, I. Pavlidis, R.I. Harrykissoon, J.F. Lucke, S. Faiz, and R.J. Castriotta. Thermal Infrared Imaging: A Novel Method to Monitor Airflow During Polysomnography. *Sleep*, 32(11):1521–1527, 11 2009.

[7] A.K. Abbas, K. Heiman, T. Orlikowsky, and S. Leonhardt. Non-contact respiratory monitoring based on real-time IR-thermography. *IFMBE Proc., Sept 7.-12.*, pages 1306–1309, 2009.

[8] F.Q. Al-Khalidi, R. Saatchi, D. Burke, and H. Elphick. Tracking human face features in thermal images for respiration monitoring. *In Proceedings of the ACS/IEEE International Conference on Computer Systems and Applications (AICCSA 2010), Hammamet, Tunisia*, pages 1–6, 2010.

[9] G.F. Lewis, R.G. Gatto, and S.W. Porges. A novel method for extracting respiration rate and relative tidal volume from infrared thermography. *Psychophysiology*, 48(7):877–887, 2011.

[10] A.K Abbas, K. Heimann, K. Jergus, T. Orlikowsky, and S. Leonhardt. Neonatal non-contact respiratory monitoring based on real-time infrared thermography. *Biomed Eng Online*, 10(1):93, 2011.

[11] C.B Pereira, X. Yu, M. Czaplik, R. Rossaint, V. Blazek, and S. Leonhardt. Remote monitoring of breathing dynamics using infrared thermography. *Biomed opt express*, 6(11):4378–4394, 2015.

[12] C.B. Pereira, X. Yu, M. Czaplik, V. Blazek, B. Venema, and S. Leonhardt. Estimation of breathing rate in thermal imaging videos: a pilot study on healthy human subjects. *J Clin Monitor Comp*, 31(6):1241–1254, Dec 2017.

[13] Y. Cho, S.J. Julier, N. Marquardt, and N. Bianchi-Berthouze. Robust tracking of respiratory rate in high-dynamic range scenes using mobile thermal imaging. *Biomed. Opt. Express*, 8(10):4480–4503, Oct 2017.

[14] FLIR Systems Inc. *Pro-Grade Thermal Cameras for Smartphones: FLIR ONE Pro-Series*, 2018.

[15] Y. Bar-Shalom and X-R. Li. *Multitarget-Multisensor Tracking: Principles and Techniques*. YBS Publishing, 1995.

[16] S. Särkkä. *Bayesian Filtering and Smoothing*, volume 3 of *Institute of Mathematical Statistics Textbooks*. Cambridge University Press, Cambridge, 2013.

[17] S. Särkkä and A. Solin. *Applied Stochastic Differential Equations*. Cambridge University Press, 2019.

[18] Z. Zhao, S. Särkkä, and A.B. Rad. Spectro-temporal ECG analysis for atrial fibrillation detection. In *2018 IEEE 28th IEEE INT WORKS MACH*, Sep. 2018.

[19] J. Fürnkranz. Round robin classification. *Journal of Machine Learning Research*, 2(Mar):721–747, 2002.